Synthesis, Designing and Sensing Applications of Nanostructured Ceria Based Materials

Sayed Tayyab Raza Naqvi,[a] Bahareh Shirinfar,[b] Saadat Majeed,[a]* Muhammad Najam-ul-Haq,[a] Dilshad Hussain,[a,c] Tanyia Iqbal[a] and Nisar Ahmed[b,c,d]*

[a]Division of Analytical Chemistry, Institute of Chemical Sciences, Bahauddin Zakariya University, Multan 60800, Pakistan

[b]School of Chemistry, University of Bristol, Bristol, BS8 1TS, United Kingdom.

[c]International Centre for Chemical and Biological Sciences, HEJ Research Institute of Chemistry, University of Karachi, Karachi 75270, Pakistan

[d]School of Chemistry, Cardiff University, Main Building, Park Place, Cardiff, CF10 3AT.

*E-mail:saadat.majeed@bzu.edu.pk (SM), AhmedN14@cardiff.ac.uk (NA)

Keywords: Cerium nanostructures; Redoxactive; Electrochemicalluminescence; Biosensor; Glucose oxidase; Catalyticactivity; Cyclicvoltammetry

Abstract

Cerium based materials possess redox properties due to their existence in dual valence states of Ce^{3+} and Ce^{4+}. In the last few years, scientific community has paid much attention to design and synthesis cerium based materials through advantageous routes for wide spread catalytic and sensing applications of the Cerium material in many fields. Cerium material has been synthesized into many different forms, shapes and sizes. Cerium nanostructure's catalytic and sensing capability is highly dependent on its morphology and can be improved significantly by modifying size and shape of nanostructures for developing sensing scaffold with improved sensing performance. These nanostructures provide basis for the applications in many fields. From literature survey (2010-2015), it is concluded that the fundamental morphologies, ratio, and capping of the Cerium nanostructures (CeNSs) constructively affects their properties and applications. Designed sensors utilizing CeNSs exhibit outstanding stability, high selectivity and eminent reproducibility in relation to time and temperature. In addition, this review will also provide a perspective insight on the future trends for designing of different morphologies of CeNSs and their promising applications.

Abbreviations: **CeNSs** cerium nanostructures; **IEP** isoelectric point; **CTAB** cetyltrimethylammonium bromide; **HMTA** hexamethylenetetramine; **ECL** electrochemical luminescence; **GOx** glucose oxidase; **MWCNT** multiwalled carbon nanotubes; **ECIS** electric cell impedance sensing; **CEA** carcino-embrynic antigen; **PSA** prostate specific antigen; **COD** chemical oxygen demand; **MG** malachite green

1. Introduction

Cerium belongs to lanthanide or Rare-Earth Elements, and is the most abundant of these Rare Earths, comprising around 0.0046% by weight in earth's crust. It has attracted much attention from researchers in physics, chemistry, biology and materials science.[1] Cerium exhibits variable electronic structure which makes it different from other lanthanides elements. The energy of inner 4f level is nearly equal to the energy of outer or valence electrons. As a small amount of energy is necessary to change the relative vacancy of these electronic levels, it mostly exists in dual oxidation states Ce^{4+} and Ce^{3+}.[2]Ce^{4+} is considered as a more stable state and coexists with its other oxidation state (Ce^{3+}). Sudden change in oxidation state is associated with its capability to store and release of O_2 designating as oxygen storage capacity (OSC). It holds fluorite like shape but phase diagram shows that CeO_2 release O_2 under reduction conditions. Although, it is reversible process and re-oxidized to CeO_2 in oxidation condition (Fig.1).[3]Unique relative stability in tetravalent state than other lanthanides, which are only stable in the trivalent state, makes Ce as a promising material. The motility of oxygen ion in CeO_2nanostructure is another vital feature for photocatalysis and electro-chemical causes.[4]Chemical and physical properties of nanocerium to bulk cerium are quite similar.

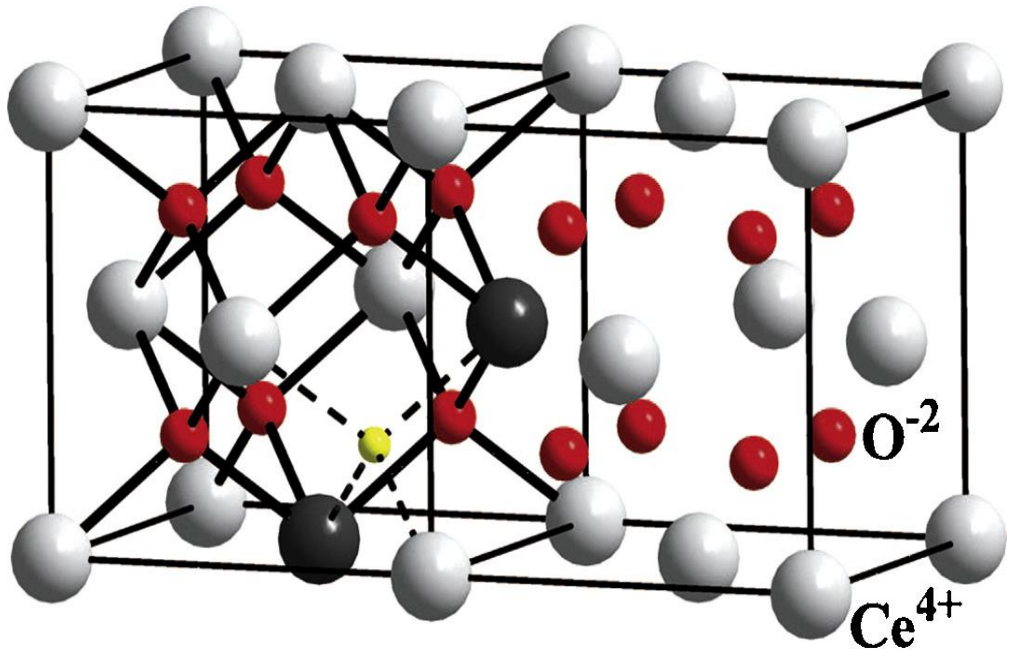

Fig.1 Fluorite like crystal of CeO_2 and O_2 vacancies.[3] Reproduced from ref 3 with permission, from the Royal Society of Chemistry, 2010.

However, nanostructures (NSs) consist of Ce^{3+}provide enhanced redox activity with respect to larger particles due to the abundance of defects and oxygen vacancies at the surface. Cerium in its oxide form was first reported in 1803and was given the name "Ceria" by Jons Jacob Berzelius in Sweden after the dwarf planet Ceres (Goddess of Agriculture).[5]The two naturally occurring forms of Cerium as carbonates (e.g., bastnasite) andphosphates (e.g., monazite) have been serving a major role for commercial uses. In oxide form as CeO_2,it adopts a fluorite crystalline structure that emerged as a fascinating nanostructured material for researchers. Cerium nanostructures (CeNSs) exist in different morphologies like nanoparticles, nanorods, nanowires. [6, 7] Ceria belongs to the transition metal oxides which have unique properties, are two dimensional (2D) in nature, have variety of application in different fields.[8]Nanocerium based peculiar analytical tools are known to be lower in cost and very sensitive owing to its especial and unique properties of high surface to volume ratio, showed outstanding selectivity, non-toxicity, high IEP (isoelectric point), high biocompatibility and thermal and chemical stability, optical and electrical activities emerging from phonon and electrical captivity.[9] CeNSs modified with a large number of nano-scaled materials like nano carbon structures, conducting nano polymer and different nano metal oxides have been immensely used for biomolecule sensing and catalytic enzyme mimetic activities.[10] Cerium nanostructure based materials have been synthesized and designed in various morphologies and sizes in order to immobilize protein, enzymes and antigens for electrochemical luminescence detection of various biomolecules for the sake of diagnosis, prognosis and biomarker study. In 2012, Chunwen Sun et al. highlighted the controlled synthesis, oxygen defects related properties and utilization of as-synthesized cerium based nanomaterial in energy and environmental applications.[11, 12] In 2013, Ceria nanoparticles were explored into research as promising therapeutic material for the treatment of cancer and diabetes.[13] While evaluative results concerning clearance, uptake and retention of these nanoparticles are incomplete and contradictory reports exist regarding in vitro toxicity.[14]In 2015, TizianaMonitini et al. published a review on catalytic behavior of cerium based nanostructures.[10]CeO_2 has been vastly investigated in various types of catalysis in the form of simple nanoparticles to variety of nanostructures and composites.CeO_2-doped lanthanides nanostrucures has been specially synthesized and deployed as catalyst in water-gas shift reactions (WGSR),[15] photocatalysis,[16] electro-catalysis[17] and in photo-degradation of volatile organic compounds (VOCs).[18] Catalytic performance of CeO_2 solely depends on disclosed surface of nanostructure.[19]Results of computer modeling has revealed that nanostructures having

100/110 planes execute excellent catalytic activities because of their high surface energies.[20]The prominent physio-chemical attributes are sensitively associated with morphology of exposed surface of nanostructures. So, it has become essential to control the designing of nanostructures to offer various morphologies for accounting structure-activity relationship. In past few years, many schemes for control synthesis have been employed to design variety of CeO_2 nanostructures from simple monodispersed nanoparticles to nanotubes, nanorods, nanocubes, nanoplates, brick and polygons.[21-23]This review provides fundamental characteristics and wide view of catalytic aspects of cerium based nanostructures those pledge to produce significant influence on our lives including basic knowledge of $CeO_2$and its properties, characterization tools, emerging traits, theoretical investigations and catalytic applications. In the last several years, cerium based materials designing have received much attention due to their applications in energy, industry, environment, and pharmaceutical.[24] In present review we tried to briefly summarize synthetic methods, designing routes and various sensing and analytical applications of cerium based nanostructure materials. (Fig.2)

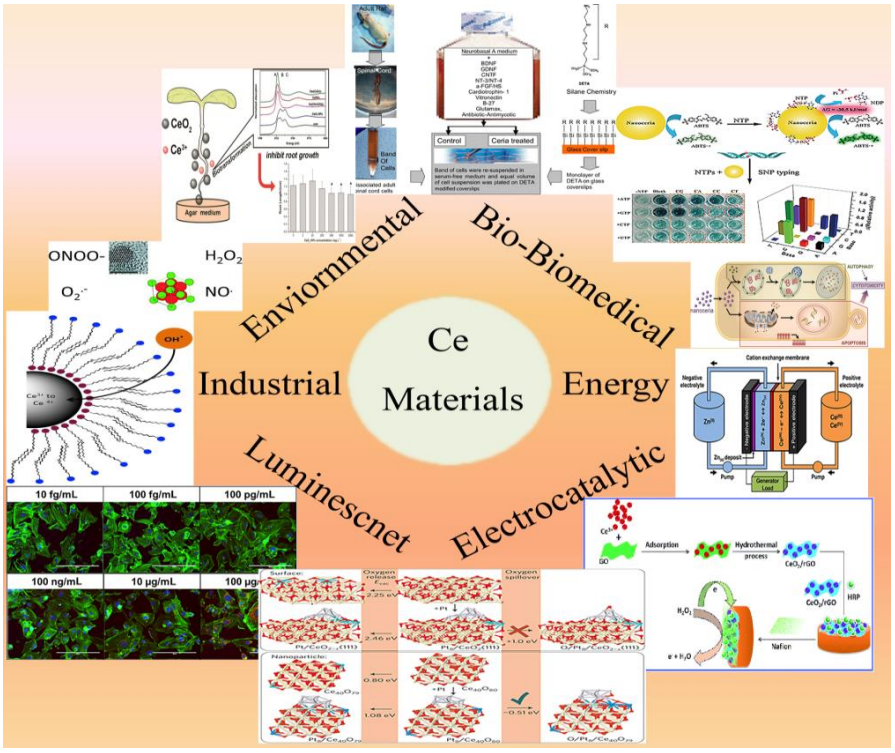

Fig.2 Cerium based nanostructured materials designing for applications.

2. Synthesis, Designing and Characterization

The controlled synthesis of CeNSs based materials is an imperative issue for environment and energy related applications. However, one major advantage of using all kinds of the nanomaterials including CeNSs is their properties that can be controlled and tailored in a conventional manner to assemble the needs of desired specific applications. Numerous techniques such as electrochemical,[25] hydrothermal andsolvothermal,[26] aqueous precipitation,[27] reversed micelles,[28] sol-gel,[29] thermal decomposition and microwave assisted protocols[30] have been adopted to synthesize CeNSs, while maintaining control of its size and properties. Moreover, various hydrophilic and hydrophobic coating of protective substances like polyethylene glycol,[31] dextran,[32] polyacrylic acid, polyvinyl pyrrolidone,[33] cetyltrimethylammonium bromide (CTAB)[34] and glucose has been used to enhance physical, chemical properties of individual bare CeNSs. Synthetic methods and designing routes are important because they determine the overall physico-chemical and optoelectronic properties including solubility, size, surface condition, charge, structural arrangement and morphology of nanoparticles.[35]

Table 1. Morphology, Methodology and Size of CeNSs

CeNS's/Morphology	**Method of Preparation**	**Reaction parameter**	**Size (nm)**	**Reference number**
Nano rods	Hydrothermal process	Annealing at 350-800^{0}C	Diameter =5-20 Length = >200	[36]
Nano particles (octahedral)	Surfactant assisted method	Add HMT (surfactant)	Smallest particle of 2	[33]
Lamellar shape	Surfactant assisted method	Ce/HEA/H_2O/EG 180^{0}C, 30 min pH 7	Width = 10 Length = 50-200	[37]
Array particles	Surfactant assisted method	Ce/HEA/H_2O/EG 180^{0}C, 24 h pH 7	2-4	[37]
Platelet rods	Surfactant assisted method	Ce/HEA/EG(30ml) 180^{0}C, 24 h pH 7	180-200	[37]

Rice shape	Surfactant assisted method	Ce/HEA/H_2O 20ml/EG 10ml 180^0C, 24 h, pH 14	6-10	[37]
Cube shape	Surfactant assisted method	Ce/HEA/H_2O 30ml 180^0C, 3 d, pH 14	40	[37]
CeO_2 crystalline powder (cubic fluorite structure)	Electrochemical synthesis	At 29^0C At 80^0C Sintered at 1300°C	10 14 350	[10]
CeO_2microcrystallites	Solvothermal method	At high temp. and high pressure	≈50	[24]
Nano-sheets **Petal shape**	Facile aqueous phase precipitation	At reaction temp. 0^0C	Thickness = 20-50	[38]
Nano-sheets **Belt shape**	Facile aqueous phase precipitation	At reaction temp. 25^0C	Length =5-10µm Width =0.5-1.2µm	[38]
Ultrafine uniform nanoparticles	Riverse micelle method	Mixing of microemulsions containing $Ce(NO_3)$ and NH_4OH	2-6	[39]
Nanospheres **Nanospheres/rods** **Nanorods**	Microwave assisted hydrothermal method	At 80^0C At 120^0C At 160^0C	About 5 5-7 Diameter = 10 length=70	[40]
Nano-octahedron	Surfactant free hydrothermal method	Addition of urea as mineralizer	200	[41]

Vertically aligned nanorods and flower like shape	Phosphate assisted hydrothermal method	$Na_3PO_{4(soln)}$ in 0.1 M[Ce^{3+}] and 0.25 M [Ce^{3+}] respectively	Width = 20-40 Length= up to several micrometer	[42]

2.1 Hydrothermal Synthesis

The hydrothermal process followed by annealing at 325°C–800°C provides single-crystalline ceria nanorods of 5-20 nm diameter. The as-synthesized CeO_2 nanorods contain high concentration of defects from oxygen vacancies and high lattice strains. The additional annealing process resulted in an improved lattice crystalline quality along with evolution of novel cavity-shaped defects in nanorods. The nanorods showed polyhedral morphologies bound by (111) and (100) surfaces. The defects usually evolved *via* agglomeration of vacancies within the as-synthesized nanorods. This systematic annealing creates true internal cavities, by diffusion of internal atomic and vacancy, and not small size and unequally distributed surface pores as reported earlier. Cubic CeO_2 nanomaterial, hydrothermally synthesized, offer high crystallinity and well exposed surface with (200) facets.[43] The systematic annealing offers new surface activity tuning route aside from previously suggested tuning by shape tuning, doping and irradiation and can be integrated with previously suggested routes. [44]

2.2 Supercritical Synthesis

In supercritical synthesis high pressure pumps are used to pump distilled water which is heated to pre-determined temperature with help of heat exchanger and pre-heater. High pressure pumps are also utilized to mix cerium nitrate ($Ce(NO_3)_3$)solution and ammonia (NH_3) solution as pH regulator with supercritical water in mixing chamber located before reactor. After mixing, final solution is kept in reactor for sufficient time period under supercritical conditions in order to synthesize cerium oxide nanoparticles. These cerium oxide nanoparticles are collected and spray dried. XRD and SEM, used to characterize the nanoparticles, revealed that nanoparticles were of heterosize ranging from 15 nm to 45 nm with heteromorphological crystalline structures.[45]

2.3 Surfactant Assisted Synthesis

Nanosized CeNSs have better performance than micron-size powder, due to larger surface to volume ratio. The small sized nanoparticles upto 2 nm are synthesized by mixing aqueous solutions of cerium nitrate and hexamethylenetetramine at room temperature for thirty minutes are single crystals having either an octahedral shape with eight (111) surfaces, or with an additional (200) surface-truncated octahedral shape. Both types of CeNSs obtained have narrow size distribution with a standard deviation less than ±15%.[46,47]The studies on exposed reactive facet-dependent catalysis of CeO_2 nanocrystals predicted that the surface reactivity on (100) facet is considerably higher than that on either (110) or (111). These properties lead to synthesize of high exposed percentage of (100) facet of ceria nanocrystals, producing a more active catalytic support. The reaction mixture of cerium nitrate/hexamethylenediamine/water–ethylene glycol produced a large number of lamellar, particle-aggregated array, platelet, rice, cube, quasi-sphere shapes of CeNSs. Studies on shape-dependent catalysis of bare ceria samples toward sensing of CO indicated that cube-shaped ceria nanoparticles show better catalytic activity than nanospheres and commercial micro powders. The shapes of CeNSs can be controlled by tuning reaction parameters. The surfactant assisted synthesis of cerium nanomaterials, using bis-amine linker hexamethylenediamine, offers intermediated sites to hybridized secondary species in order to synthesize hybridized nanomaterials with high oxygen carrying capacity. [48]

2.4 Capping Agent Assisted Synthesis

The nanoparticles size, during the synthesis and procedure adopted, play a significant role in sensing and catalytic activities. A slight change in synthesis composition and condition leads to totally different nanostructure. The initial precursor's type, capping agent and precursor's ratio determine the overall properties of CeNSs.CeO_2 nanostructures synthesized using hexamethylene-tetraamine (HMTA) and fructose as a capping agents show rhombohedral/cubic particles and spherical shapes, respectively. The average diameter of the NPs found to be6.4 nm and 5.8 nm.CeO_2-HMTA, due to the better exposure of the active (200) and (220) planes relative to (111) plane, exhibits superior electrocatalytic activity. [49] Moreover, on the other side, use of oleic acid and oleate negatively charged ion as capping agent form nanocubes whose morphology could be altered by varying cerium's initial concentration. The number of surface oxygen vacancies highly affects catalytic properties of CeNSs. The higher oxygen and electron vacancies are directly related to higher ratio of Ce^{3+}/Ce^{4+}in nanoparticles preparation and thus alter the properties of as

synthesized materials. Role of capping agents, in the synthesis of ceria nanoparticles, is to control the size uniformly but capping agent synthesis required high concentration of cerium salt. [50, 51]

2.5 Microwave Assisted Synthesis

The microwave-assisted method with varied temperature conditions proved to be highly efficient for synthesis of CeO_2 nanoparticles with a large number of structural defects. The samples synthesized at 80 °C consisted of spherical particles of about 5 nm, while those synthesized at 120 °C presented a mix of spherical and rod-like nanoparticles and the sample synthesized at 160 °C consisted of nanorods with 10 nm average diameter and 70 nm length. The presence of structural defects is attributed to an associated reduction in the valence of Ce^{4+} ions to Ce^{3+} ions caused by the increasing molar fraction of oxygen vacancies at assorted temperature. In this type of synthesis, microwave irradiation enhances the generation rate of anisotropic CeNSs with variety of morphology regulated by the oriented attachment (OA) growth mechanism. [30]

2.6 Precursor and Activator Assisted Synthesis

During synthesis, initial precursor's types controls the CeNSs morphologies and catalytic characteristics, acting as capping agent and oxidizer as well. The anionic composition or the type of counter ion of Ce^{n+} such as chloride, nitrate and phosphate in solution before any further treatment controlled the shapes of CeNSs. [52]These anions exhibited selective interaction with specific facets of CeO_2, leading to the growth of CeNSs with varying morphologies consisting of nanospheres, nanowires, and nanorods. Usually phosphate and chloride ions are shown to play critical roles in obtaining high aspect ratio CeNSs. $CeCl_3$ as a cerium precursor produces pure nanorods using a wide range of synthesis compositions and conditions. It was suggested that halide anions can absorb onto surfaces of initial $Ce(OH)_3$ nuclei and stabilized the shape. In contrast, presence of oxidizing anions like $NO_3^-$and SO_4^{2-} as a precursor source gradually convert one nanostructure into another making it unstable for further use. [52-55,56]The presence of phosphate ions in concentration dependent manner is an important key in most of the cases in preparing CeO_2nanorods. The PO_4^{3-} produces pure nanorods upto 1×10^{-3} M concentration. However, on raising phosphate concentration ion above 1×10^{-2} M, cerium phosphate impurities often started to appear in final CeNSs product and limits its applications. Fascinating precursor and activator assisted hydrothermal synthesis of CeNSs is cheap and simple which make scheme promising for other faceted nanomaterials. [57]

2.7 Template Free Hydrothermal Synthesis

In template and surfactant free hydrothermal synthesis cerium nanomaterials are synthesized by 30 min stirring of solution of 12.5 mL 28% ammonia solution and 0.5M cerium nitrate or cerium chloride after stirring precipitates are washed with ammonium nitrate (NH_4NO_3) or ammonium carbonate ($(NH_4)_2CO_3$) before undergoing the hydrothermal treatment. Unlike techniques and procedures that require the use of organic and inorganic additives or templates, surfactant- and template-free solution precipitation along with hydrothermal treatment represents a simple yet effective means to fabricate CeO_2nanowiresornanoparticles. The nanostructures possess the potential to be further tuned to provide a morphologically controllable route for tailoring and designing CeO_2nanomaterials for a wide variety of applications. [53]It is well-known that the use of chemical additives and successive removal process may contaminate CeNSs and influences possible applications or biological responses, and therefore, should be avoided. The most commonly used strategy to prepare Ce nanostructures in a template-free system is to mix Ce^{3+}salt with high concentration of alkaline solution without any additive, leading to the formation of CeNSs with nanorod nuclei. These rod-like $Ce(OH)_3$nanocrystals further can be converted to CeO_2 without any shape change. [54, 58]

2.8 Phosphate Assisted Synthesis

In contrast to template free synthesis, Xing and co-workers[59, 60]established a procedure for the synthesis of CeNSs under acidic conditions using a very small amount of sodium phosphate ($Na_3PO_4.6H_2O_2$) as a mineralizer (Fig.3). The as synthesized nanostructures provide better dispersion and narrow size distribution than alkaline conditions. Additionally, in presence of phosphate, morphologies of hierarchical architectures can be selectively produced by adjusting Ce^{3+} ion concentration.

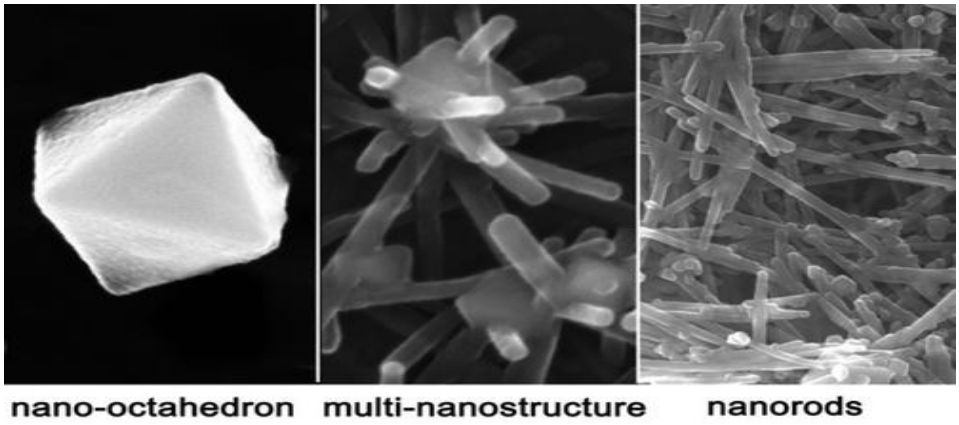

Fig.3 Template-free hydrothermal synthesis of CeO_2 nano-octahedrons and nanorods.[60] Reproduced from ref. 60 with permission from American Chemical Society, 2008.

The flower-like and vertically aligned nanorods morphologies could be obtained at Ce^{3+} ion concentrations of 0.25 M and 0.1 M, respectively. Generally, phosphate ions in reaction controlled overall morphologies of CeO_2 nanostructures by controlling electrostatic potential and surface energy of CeO_2nanorods. (Scheme: 1)

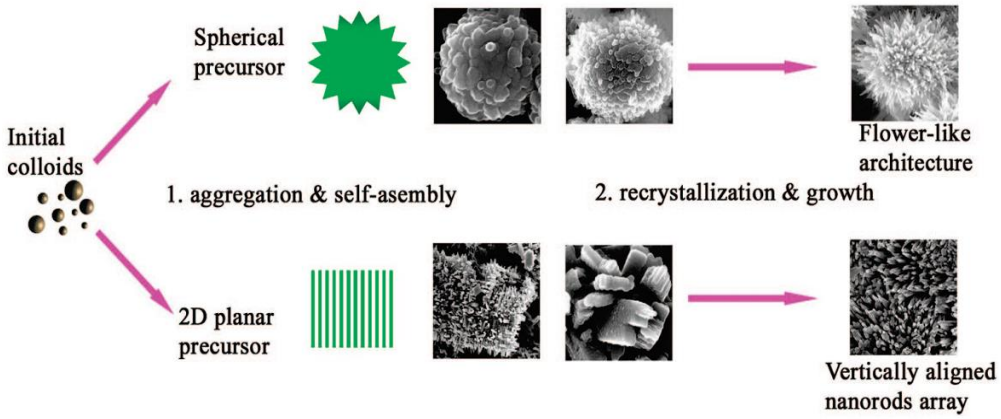

Scheme: 1 Schematic illustration for the formation of the ordered CeO_2nanorods hierarchical architectures. [59] Reproduced from ref. 59 with permission from American Chemical Society, 2008.

Since different morphologies effect the overall properties of CeNSs materials, these can be obtained by carefully adjusting the synthesis conditions such as precursor concentration, temperature and synthesis time. CeO_2 nanowires show higher catalytic activity for CO oxidation and oxygen storage capacity than nanorods and nanoparticles. SiandFlytzani-Stephanopoulos observed a strong shape/crystal plane effect of CeO_2 on the gold–ceria activity for the water-gas shift reaction. The rod-like ceria enclosed by (110) and (100) planes offers the most active surfaces for gold stabilization and activation. In this synthesis, addition of phosphate could assist regulate shapes of CeNSs by regulating cerium oxide nanorods surface energy and electrostatic potential. [61]

2.9 Co-Precipitation Method for Synthesis

The co-precipitation synthesis takes edge of simplicity and low solubility coefficients, utilized as commercial method for synthesis. The CeO_2nanoparticles are synthesized in the range of 2-8 nm via co-precipitation method using NaOH,[62] urea[63] and ammonia[64] as precipitating agent. The size and shape of nanoparticles can be tailored by varying reaction parameters as rod-like particles and spherical shaped particles are synthesized when oxidized by H_2O_2 at pH 8 and lower than pH 7, respectively. This method of synthesis is propitious route to regulate the size and morphology of nanomaterials.

2.10 Electrodeposition Method of Synthesis

Eu-doped CeO_2 nanosheets are synthesized by preparing the solution of nitrates of europium, cerium and ammonium in concentration of 0.01 M, 0.001 M and 0.1 M, respectively. It is kept at -0.2 mA for 60 mins at 70 ºC. Different concentration rang (1% - 8%) of dopant are doped with this method. In order to remove impurities, washing is done by distilled water and dried for 24 hrs. As-prepared nanorods are annealed at 550 ºC for 60 mins. Resultant Eu-doped CeO_2 nanosheets (Fig.4) can be easily tailored by varying the percentage of Eu in Ce.[65]

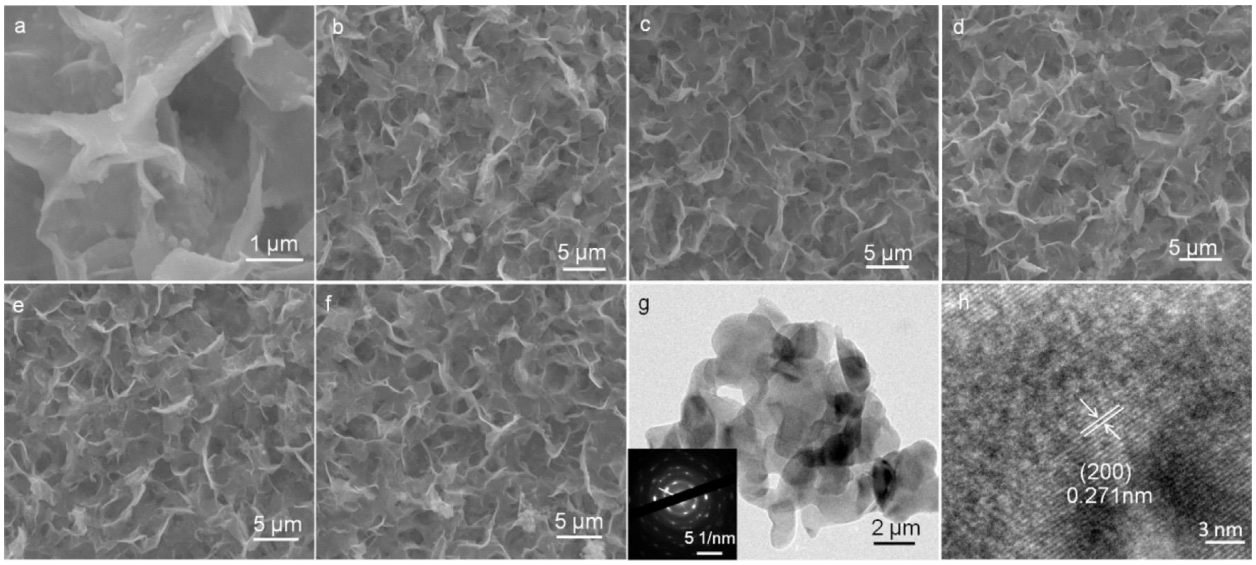

Fig.4 SEM of the (a) 4% Eu/CeO_2nanosheets, (b) CeO_2nanosheets, (c) 1% Eu/CeO_2nanosheets, (d) 2% Eu/CeO_2nanosheets, (e) 4% Eu/CeO_2nanosheets, and (f) 8% Eu/CeO_2nanosheets. (g) TEM image and SAED pattern of the 4% Eu/CeO_2nanosheets. (h) HRTEM image of 4% Eu/CeO_2nanosheets. Reproduced from ref. 65 with permission from Elsevier, 2016.

CeO_2 nano-octahedrons (Fig.5) were synthesized by galvanostatic electrodeposition comprising F-decorated-SnO_2-glass as working electrode, rod of graphite as auxiliary electrode and Ag/AgCl as reference electrode. All electrodes were dipped in solution of cerium nitrate and dimethyl-sulfoxide in water.[66]

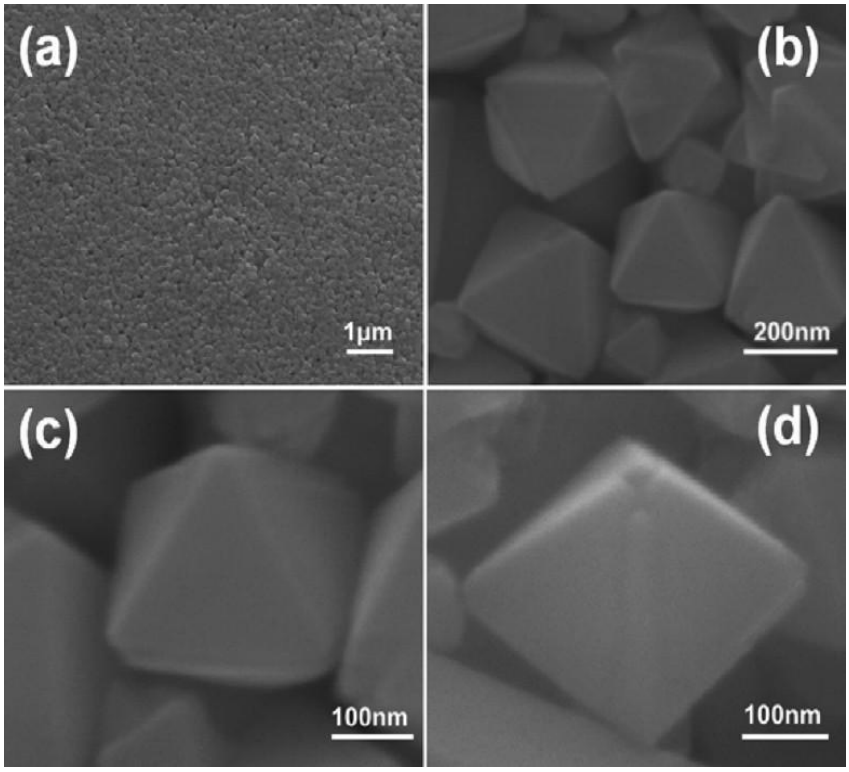

Fig.5 SEM images of CeO_2 nano-octahedron. Reproduced from ref. 66 with permission from American Chemical Society, 2010.

Spherical and needle shape core shell nanostructures were electrochemically synthesized by electrophoretic deposition (EPD). To synthesize ceria based nanostructures, polystyrene based scaffold (working electrode) was dipped in two different concentrations, 10 and 1 mM, $Ce(NO_3)_3$ solutions. As concentration of $Ce(NO_3)_3$ was changed from 10 mM to 1 mM, the shape changed from spherical core shell to needle like porous core shell (as shown in fig 6).[67]

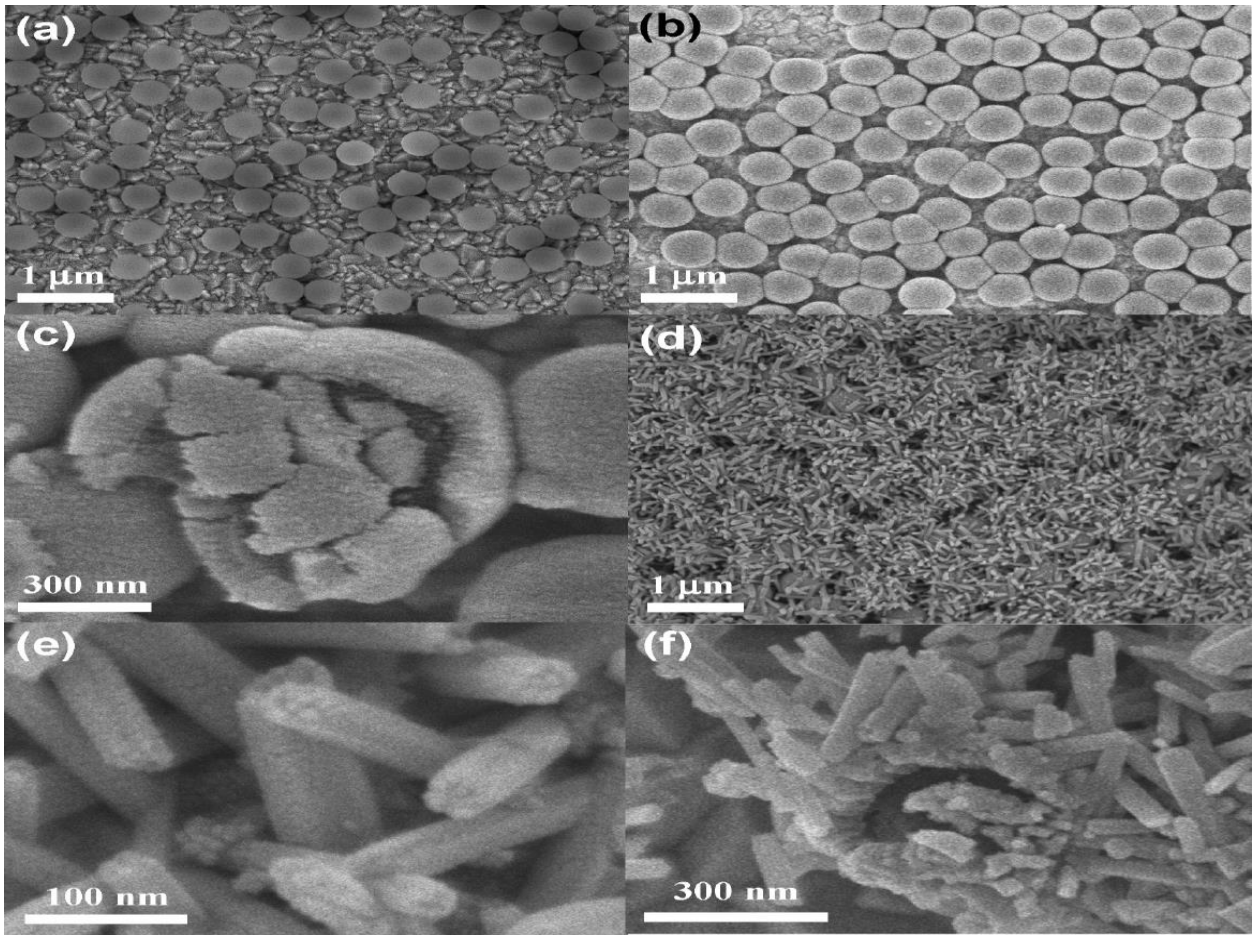

Fig 6. SEM images of Spherical and needle-like Ceria based core shells.[67] Reproduced from ref. 67 with permission from American Chemical Society, 2009.

Sensing activity of ceria based nanostructures can be further elevated, specifically at low temperature, by regulating their size and morphologies.[68] Electrochemical synthesis of nanostructures can easily be executed at ambient temperature, which offers great control on size and morphology of as-synthesized nanostructures.

3. Structure Activity Relationship of Ceria

CO_2 generation from the oxidation of CO is based on energy required for oxygen extraction from nano ceria catalyst.[69] Lower the energy required for extraction, more the catalytic activity towards oxidation. No doubt, energy required to generate oxygen positions on nano ceria catalyst has seemed to be simple but promising tool to predict catalytic behavior of ceria based nanostructures.[70] It was determined that it is facile to obtain oxygen from ceria nano-catalyst

possessing {310}, {110} and bipolar {100} facets relative to containing {111} facet. However, these active facets show less thermal stability as compared to {111} facet. Synthesis of ceria based structures at nanoscale offer active ceria facets as compared to bulk size ceria; particularly ceria nanostructure possess a high weight age of {110} and {100} relative to {111}. Additionally, ceria nanocubes, comprising six {100} active facets, have been engineered by regulating synthetic protocol and parameters.[71] Specially, energy required to extricate oxygen from ceria based nanomaterials was estimated to be highest for bulk (+623 KJ per mole) and lowest for {100} (+51 KJ per mole). Consequently, catalytic activity of ceria based nanostructures can be modified, controlled and enhanced through generating oxygen defects.[10] It was also unveiled from the further investigations that activity respecting oxidation shows minimum by ceria based mesoporous nanocubes and maximum by small sized ceria nanoparticles. It means that the small nanoparticles, possessing {100} facets, needed less amount of energy to withdraw the oxygen rather than other nanostructures. Moreover, it was also disclosed that oxygen is depleted as oxidation precede upto 10%; the maximum depletion reached. But this was not true in the case of smallest nanoparticles of 3.5 nm which did not exhibit maximum oxygen depletion of 10% rather it showed easy oxygen extraction at 2%.[72] This oxygen deficiency was restored via reduction of NO_2 to NO. All of these studies of structure-activity relationship were furnished with the help of molecular dynamic simulation (MD simulation). MD simulation was employed to develop atomic models of various ceria based nanomaterials possessing various structures. These atomic models were deployed to estimate energy concerned with ceria nanostructures to catalyze the oxidation (CO to CO_2) and reduction (NO_2 to NO). Peculiarly, energy regarded with creation of oxygen defects was estimated, which has been pretended to be simple but promising tool to predict the catalytic activity on ceria nanostructures. These calculated activity results was deployed to control the experiment. As, size, numbers of defects and engineering of various shapes are playing a key part in driving the catalytic activity. Conclusively, defects generation on ceria based nanostructures can easily be regulated finely, during synthesis reaction, by exposure to oxidizing or reducing ceria nanostructures.[73]

4. Sensing Applications of Ceria

The formation of cerium aqueous complexes and solubility products involve binding of a metal center(Ce^{3+} or Ce^{4+}) to other ligands and organic molecules to form a coordination complex. These complexes' ability is utilized in the screening, sensing and investigating various sensing

applications in many fields. In following sections, we have reviewed wide range of electrochemical, luminescent, fluorescent, biomedical and gas sensors. [74-76]

4.1. Nano-Enriched Electrochemical and ECL Sensing

Novel analytical devices based on cerium nanostructured metal oxides are known to be cost-effective and highly sensitive due to large surface-to-volume ratio and excellent selectivity. Electrical conductivity, good catalytic activity, large surface area, chemical stability, adsorption, nontoxicity, and biocompatibility make CeNSs promising material to fabricate electrochemical biosensor. Microenvironment and synthesis method adopted also plays an important role in determining the activity of CeNSs. For example CeO_2 nanowires show higher catalytic activity for CO oxidation and oxygen storage capacity than nanorods and nanoparticles. CeNSs sensors possess unique regenerative properties owing to their low reduction potential and co-existence of both Ce^{3+}/Ce^{4+} on their surfaces. The surface of sensors is influenced by Ce^{3+}/Ce^{4+} ratio and microenvironment. Defects in crystal lattice due to the presence of Ce^{3+} play an important role in tuning redox activity of CeNSs. [77, 78]Ability of cerium oxide to act as a redox couple makes it a promising material to act as a matrix for the fabrication of a mediator-less amperometric biosensor. Further, owing to its high isoelectric point (IEP) ~9.0, CeO_2 is suitable for adsorption of enzymes having low IEP like glucose oxidase (GOx) having IEP 4.2, [79]without any harsh chemical treatment.

In 1967, first GOx enzyme based glucose biosensor was prepared by Hicks and Updicks. From then, continuous research has been done to develop GOx enzyme based biosensors in order to impedimetric, conductometric, potentiometric, amperometric sensing of glucose.[64, 80, 81] A successful attempt have been made towards the fabrication of a mediator-less amperometric glucose biosensor by immobilization of GOx enzyme on the nanoporous surface of CeO_2 thin film. These films are deposited on platinum coated glass slide using pulsed laser deposition technique. Response studies carried out on bio-electrode using differential pulsed voltammetry and optical measurements show linearity in range of 25–300 mg/dL of glucose. The linear increase in oxidation current at 0.33 V with increasing glucose concentration upto 300 mg/dL indicated the potential of CeO_2 matrix for realization of a mediator-less biosensor. The relatively low value~ 1.01mM of Michaelis-Menten constant and longer shelf life upto 10 weeks showed enhanced enzymatic activity and stability of glucose oxidase onto CeO_2/Pt surface. [82]Likewise,

nanostructured-cerium oxide film covered by co-immobilized urease and glutamate dehydrogenase worked as a bio-electrode for detection of urea in analytical samples. The particle size of nano-CeO_2film was about 23 nm. The film was deposited onto an indium-tin-oxide coated glass substrate by dip-coating via sol-gel process. Electrochemical response of bioelectrode is found to be sensitive in 10–80mg/dL and can detect urea concentration to 0.1 mg/dL level. [83]

The nanoCeO_2 particles provide an increased electro-active surface area for the loading of analytes with desired orientations, resulting in enhanced electron communication between analyte and electrode. Rabbit-immunoglobulin antibodies and bovine serum albumin immobilized onto sol-gel-derived nanostructured cerium oxide film fabricated onto an indium-tin-oxide (ITO) coated glass plate gives electrochemical response for detection of ochratoxin-A. The nano CeO_2/ITO immune electrode exhibits improved characteristics for linear range (0.5-6 ng/dL), low detection limit (0.25 ng/dl), fast response time (30 s) as well as high sensitivity (1.27 µA/ng.dL.cm^2). [84]Excellent electronic conductivity makes CeNSs an attractive matrix for biosensor application However, CeO_2 sometimes suffers from the low electron conductivity, which seriously affects their electrocatalytic efficiency. To overcome the shortcoming, cerium oxide coated multiwalled carbon nanotubes (CeO_2@MWCNTs) and nonporous CeO_2 thin films have been constructed to improve the conductivity and surface-to-volume ratio to detect biological important molecules. [82, 85, 86] GO/MWCNTs-COOH/Au@CeO_2 serves as highly sensitive label-free ECL immunosensor for detection of carcino-embryonic antigen (CEA) where CeO_2 nanoparticles were exploited as an ECL luminescent material. The proposed ECL immunosensors constructed on the antigen-antibody specific recognition. The electron transfer could be hindered by the proteins and the ECL response in turn decreased with the increase of concentrations of CEA (Fig.7). [87]

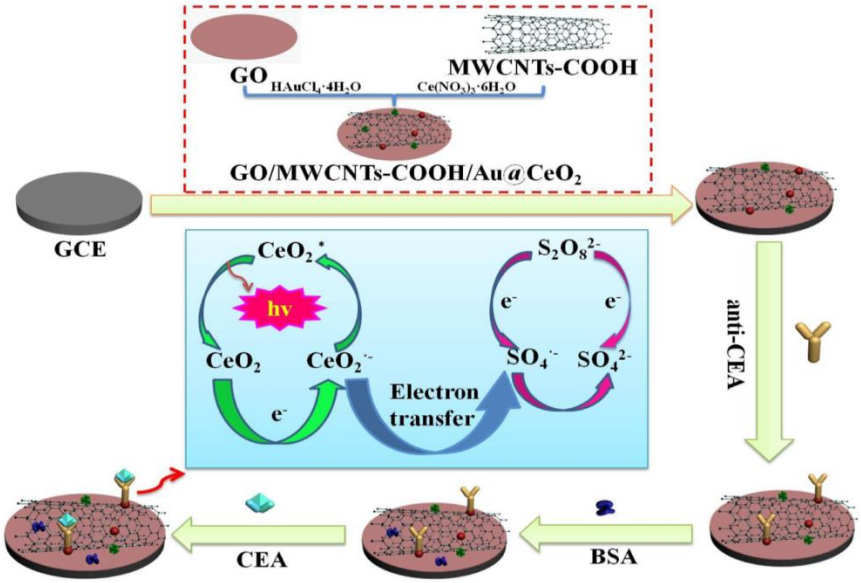

Fig.7 Fabrication of label-free ECL immunosensor. [87] Reproduced from ref. 87 with permission from American Chemical Society, 2015.

The catalytic activity of ceria mesoporous spheres in aqueous media makes them a powerful tool for a wide range of potential applications in bioassay and biological areas. The large surface area of CeNSs is likely to provide a better matrix for the immobilization of desired analytes, leading to an increased loading per unit mass of nanoparticles. A three dimensional (3D) architecture was fabricated by combining multiwall carbon nanotubes and CeO_2 mesoporous spheres using the layer-by-layer method and electrochemical immunoassay was used for sensitive detection of prostate specific antigen (PSA).The CeO_2 mesoporous spheres and excellent conductivity of MWCNTs, together impart highly suitable microenvironment for effective antibody immobilization, high stability and bioactivity. [88]CeNSs decorated graphite felt (GF) composites have been applied as high performance electrodes material for vanadium redox flow batteries. The electrode decoration with CeNSs significantly improved the electrochemical activity of pristine graphite felt. SEM and X-ray Diffraction study showed homogeneous dispersion of nano-ceria on GF.CeO_2/GFs exhibits higher activity and better reversibility towards the VO^{2+}/VO^{2+} redox reaction (Fig.8) compared with the pristine graphite felt. The vanadium redox flow batteries single cell analysis indicated that CeO_2/GF (0.2 wt%) showed the highest energy efficiency of 64.7% at the current density of 200 mA cm^2, which is significantly higher than that of the pristine GF

(53.9%). Furthermore, the cycle life test demonstrated outstanding stability of the CeO_2/GFs electrode. [89]

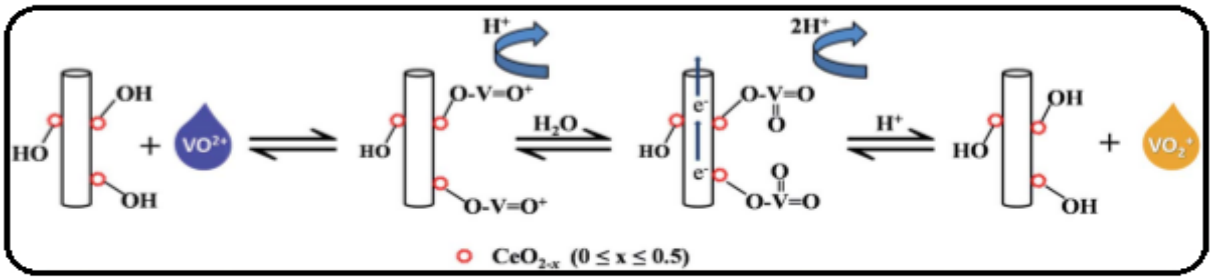

Fig. 8 The anticipated redox mechanism on CeO_2/GF electrode regarding VO^{2+}/VO_2^{+}. Reproduced from ref 89 with permission from the Royal Society of Chemistry, 2014.

CeO_2 showed attractive sensitizing effect on ruthenium bipyridine-tramadol{Ru $(bpy)_3^{2+}$-tramadol}electrochemiluminescence system. Under optimal conditions for Ru$(bpy)_3^{2+}$-tramadol system, a linear relationship between the ECL intensity and concentration of tramadol in the range of 1.0×10^{-10} to 2.5×10^{-8} mol/L exist with detection limit of 9.0×10^{-11}mol/Land relative standard deviation of 2.9%(S/N=3).The larger charging currents at CeO_2-Ru $(bpy)_3^{2+}$-carbon paste electrode was attributed to increase in electrode surface area due to the presence of CeO_2 nanoparticles. CeNPs increases surface area, and enhance electrocatalytic activity by redox behavior of Ce^{4+}/Ce^{3+}.The redox behavior significantly catalyze the oxidation of Ru$(bpy)_3^{2+}$ to Ru$(bpy)_3^{3+}$.[90] Electrochemical studies of uric acid have been an active area of research in recent years.[91] It is the final metabolic product of purine nucleotide catabolism in humans, and abnormal levels of uric acid are symptoms of several diseases such as gout and hyperuricaemia CeNSs as an elctro-active substrate material like nanoceria have been used to modify glassy carbon electrodes, made distinctive by cyclic voltammetry (CV) and electric cell-substrate impedance sensing (ECIS), for sensitive and selective determination of uric acid in analytical samples. In mild acidic buffer of pH 6.0, CeNSs modified electrode showed outstanding electro-catalytic activity for the oxidation of uric acid (UA). The catalytic current produced at the electrode surface has good linear relation to uric acid in the range of 2.0×10^{-7}-5.0×10^{-4}mol/L with detection limit of 1.0×10^{-7}mol/L and correlation coefficient of 0.9986. [92] Cerium doping grants higher electro-catalytic response and shelf life. The increase in cerium atomic proportion in nano-composites electrodes increases electro-active property of Ce-doped electrodes. Ce-doped PbO_2electrodes retains increased oxygen

evolution over potential (1.98 V) than PbO_2 electrodes (1.51 V) and Ce-doped PbO_2 electrodes with the storage life of 135 hours. [93] As synthesized CeO_2 nanocubes dispersed on exfoliate graphene offered outstanding electrochemical sensing of UA. As prepared electrode exhibited 30 times more electrochemical sensing than pristine CeO_2 modified electrode.[43]

4.2. Nano-Enriched Sensing for Bioanalytical Applications

CeNSs are well-known as catalysts and possess astonishing, attractive and potential pharmacological, biological and medical applications due to their antioxidant properties.[94, 95] These are well known to exhibit the free radical scavenging properties by reversible binding and shifting between the reduced (Ce^{3+}) and oxidized (Ce^{4+}) forms at the particle surfaces. Ce^{o} exist in Ce^{4+} valence state, have a great efficiency to absorb oxygen and co-exist with the reduced form (Ce^{3+}).[96, 97]The shifting between the two states makes CeNSs as a promising, biocompatible and attractive platform for the biological systems and applications. These have been tested and widely used in both animal and cell culture models to determine its ability to protect against oxidative stress. [98-100]

CeNSs have been reported to exhibit activity to protect the cells from many reactive oxygen species like superoxide and hydrogen peroxide. They have been reported to shows significant superoxide dismutase (SOD)–mimetic activity[101]and catalase–mimetic activity[77]in cells.[71]It catalyzes the disproportionate of superoxide to H_2O_2 and O_2 in two steps as follows.

$$M^{n+1}\text{-SOD} + O_2^{\bullet -} \longrightarrow M^{n+}\text{-SOD} + O_2$$

$$M^{n+}\text{-SOD} + O_2^{\bullet -} \longrightarrow M^{n+1}\text{-SOD} + H_2O_2$$

The valence switch ability of CeNSs makes it possible for these materials to be used as a SOD mimic. [102]Normally, oxidative stress is a condition when the concentration of free radicals and reactive molecular species rise above certain level in living systems. This condition not only perturbs the normal physiology of the system but also has been implicated in many diseases in humans and other animals. Hydrogen peroxide is known to be involved in induction of oxidative stress and has also been linked to a variety of ailments such as inflammation, rheumatoid arthritis, diabetes, and cancer in humans. CeNSs has been synthesized using different capping agents; Hexamethylenetetraamine and fructose. Both the NPs showed the excellent amperometric

response to the hydrogen peroxide with a sensitivity down to 21.13 and 9.6 $\mu A\ cm^{-2}\ mM^{-1}$ for hexamethylene-tetra-amine and fructose based materials, respectively.

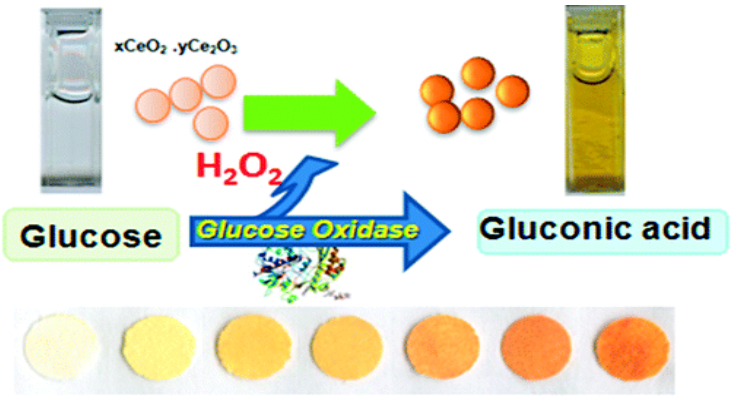

Fig.9 Paper bioassay based on ceria nanoparticles as colorimetric probes[103] Reproduced from ref. 103 with permission from American Chemical Society, 2011.

CeNSs work as chromogenic indicators in colorimetric probes in response to the analyte based on the changes in the physicochemical properties of ceria nanoparticles. Ceria nanoparticles co-immobilized with glucose oxidase onto filter paper using a silanization procedure detect enzymatic hydrogen peroxide efficiently produced in a concentration-dependent manner. The assay (Fig.9) is fully reversible and can be reused for consecutive measurements without significant loss of activity. [103]Similarly, CeO_2 NPs exhibit intrinsic peroxidase-like activity, which can catalyze the oxidation of 3,3',5,5'-tetramethylbenzidine in presence of $H_2O_2$to produce blue reaction.(Fig.10) [104]

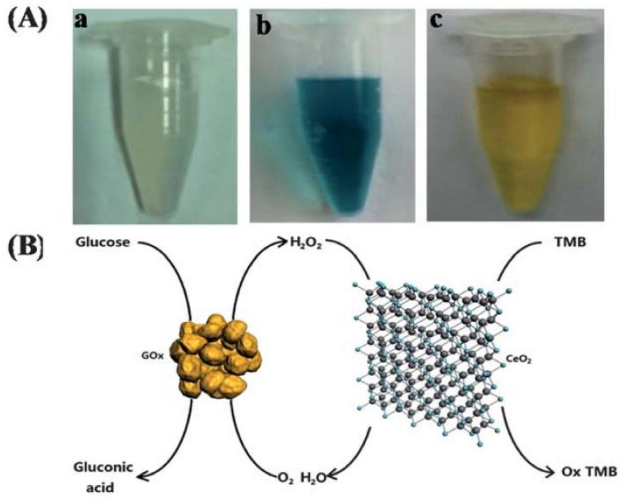

Fig.10 (A) Images of the solution of CeO_2 NPs redispersed in water (a) mixture of TMB@2HCl and H_2O_2 after catalytic reaction by CeO_2 NPs (b) mixture of TMB@2HCl and H_2O_2 after adding H_2SO_4 to quench the catalytic reaction by CeO_2 NPs (c). (B) Schematic illustration of colorimetric detection of glucose by using glucose oxidase (GOx) and CeO_2 NPs catalyzed reactions. [104] Reproduced from ref 104 with permission from the Royal Society of Chemistry, 2012.

The Ce^{3+} self-doped ceria-based CeO_2:Tb^{3+}, Ce^{3+} nanoparticles offer luminescence tunable platform for many analytes. The excess Ce^{3+} ions give rise to energy transfer from Ce^{3+} to Tb^{3+} in nanoparticles and show tunable green luminescence, a long lifetime and low photo bleaching in water. The luminescence intensity of CeO_2:Tb^{3+}, Ce^{3+} nanoparticles is sensitive to H_2O_2 concentrations due to the high ratio of Ce^{3+}/Ce^{4+} in ceria. The gradual quenching of emission intensity of nanoparticles can be recovered by treating with ascorbic acid. The on-off luminescence cycling reveals good anti-fatigue properties of CeO_2:Tb^{3+}, Ce^{3+}nanoparticles (Fig.11). [105]

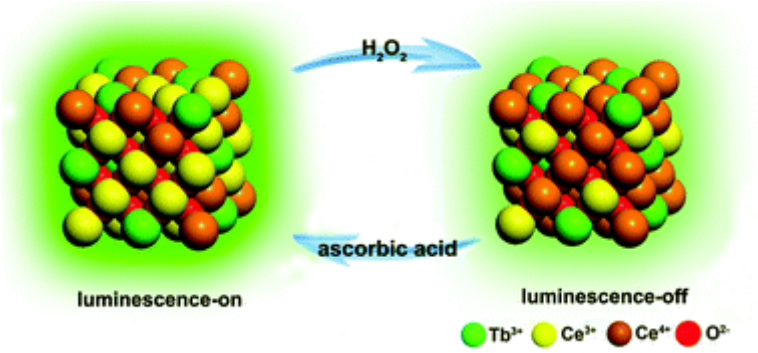

Fig.11 Self-doped Ce^{3+} enhanced CeO_2 host matrix for energy transfer from Ce^{3+} to Tb^{3+}.[105] Reproduced from ref 105 with permission from the Royal Society of Chemistry, 2013.

CeNSs are the potential antioxidant agent *in vivo* and *in vitro*, because of very attractive features such as high biocompatibility and possibility to regenerate initial oxidation state through redox cycling reactions. [49, 106] CeNSs protect cells from oxidative damage, radiation damage, oxidative stress and inflammation. [99] In a study, nanoceria was injected into transgenic mice expressing monocyte chemo-attractant protein-1 in the cardiac tissue. These mice develop myocardial inflammation leading to fatal ischemic cardiomyopathy. [107] Nanoceria injection relieved many clinical symptoms of transgenic mice, possibly due to its radical scavenging properties that reduce inflammation. [108, 102] Moreover, nanoceria reduced ROS production and apoptosis induced on H9c2 cardio-myoblasts cultured in high glucose levels to mimic diabetes conditions. [98]

The oxidase-like activity of nanoceria can be tuned by changing pH of the solution, facilitating the mild oxidation of a substrate to yield a product with enhanced fluorescent properties. The CeNSs oxidizes ampliflu at pH 7 to fluorescent product resorufin, without further oxidizing the substrate to non-fluorescent product resazurin (Fig.12). This unique capability of nanoceria is due to its mild oxidizing activity at neutral pH that prevents further oxidation of substrate to resazurin in the absence of hydrogen peroxide. In order to detect the cancer biomarker, on the basis of above results, CeNSs surface immobilized antibodies conjugated with protein G to identify the expression of epithelial cell adhesion molecule (EpCAM) and folate receptor from the patients suffering from breast carcinoma and lung carcinoma cells, respectively. Conventional enzyme-linked immunosorbent assay(ELISA) had higher displaying time of 15 hours, higher detection

limit and multiple washing steps at the same time as CeNSs detect the expression of folate and EpCAM within 3 hours. In the light of results and CeNSs's capability to oxidize ampliflu to stable fluorescent product at pH 7.0, the utilization of antibody immobilized CeNSs in the lab and molecular diagnosis is predicted. The selective nanoceria-mediated oxidation of ampliflu could be used to develop sensitive cell-based ELISA, offering various advantages over the conventional HRP/H_2O_2 ELISA.[109,103]

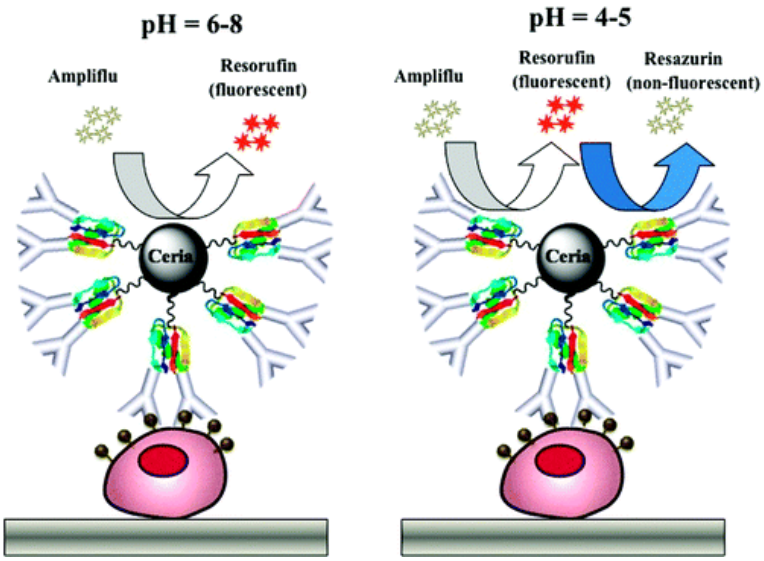

Fig 12. The capability of CeNSs to oxidize ampliflu on various pH. Reproduced from ref. 109 with permission from American Chemical Society, 2011.

Reversible phosphorylation and dephosphorylation mechanism in the living cells is involved in regulation of gene expression and protein synthesis, which controls cell growth, division or differentiation. [110-112] CeNSs has been reported to show a high efficiency in phosphopeptides enrichment as well as in dephosphorylation. These nanostructures provide true compatibility and enhanced overall working efficiency in composites with Fe_2O_3 and SnO_2.The enrichment/de-phosphorylation effect of ceria-nanocomposites provides a route to identify protein phosphorylation as well as to work at lower detection limits for biomarker discoveries. [113] CeNSs demonstrates a range of activity in human cells as well. Unlike other microorganisms, effective uptake of CeO_2 by human cells has been investigated frequently. These nanomaterials modulate

brain-derived neurotrophic factor pathway in human Alzheimer's disease models in order to trigger neuronal survival. [114]

Cerium oxide nanoparticles play important roles in antimicrobial resistance detection by shift in absorbance. Madero-Visbal *et al*., [115] recently suggested that CeO_2NPs reduces dermatitis and skin hyperpigmentation in cells exposed to ionizing radiations. Moreover, these NPs protect gastrointestinal epithelium from radiation-induced damage through reduction of reactive oxygen species and by upregulation of superoxide dismutase. [116] Ischemic stroke is leading cause of adult disability is one of the leading cause of death worldwide. The optimal doses of CeNPs in living animals found to reduce ischemic brain damage. The nanoparticles target the damaged area by disruption of blood–brain barrier after ischemia making CeNPs more chemically potent and biologically compatible materials. [117]

4.3 Nano-Enriched Sensing for Environmental and Industrial Applications

CeNSs offers most promising nanostructures scaffolding for carbonic anhydrase inhibitors, [118,119] and as an oxygen sensor[101] due to its oxygen storage capability, adequate sensitivity and low-cost synthesis. It is a potent candidate in free radical scavenging, in sensing and quantifies peroxide levels, and in real time monitoring of dissolved oxygen [120] because of its unique redox properties.

Ce-doped PbO_2 electrodes possess higher oxygen evolution over potential (1.98 V) than PbO_2 electrodes (1.51 V) and Ce-doped PbO_2 electrodes. The shelf-life of nanocomposites electrodes is 135 hours. The increase of atomic percentage of cerium in the nanocomposites electrodes increases electrocatalytic behavior of electrode.[121] The malachite green(MG) and chemical oxygen demand (COD) elimination efficiency of cerium doped PbO_2 has become 95.4% and 69.3%, respectively, with 30mA/cm^2 current density at pH 5.0.Ce-doped PbO_2 showed highest COD elimination efficiency and decreased energy dissipation with downgrading of MG.Pd-CeO_2 nano-catalyst shows excellent catalytic activity for degradation of lignite, humic acid and also water humic acid which is responsible for health hazards.[122]3D-CeO_2 nanocubes is compared with 1D-CeO_2 nanorods for catalytic degradation of aryl alcohols and alkanes for which nanocubes proved to be excellent catalyst at green conditions as possessing efficient uniform {100} facets.[123] During several years, CeO_2, CeO_2 based nanostructures and their rare earth metal oxide have attained the extreme attention as catalyst and as electronic and morphological stimulator in heterogeneous

catalytic processes.[124] So, CeO_2 based nanomaterials are being studying as sensor for gases like NOx,[125] COx,[126] H_2,[127, 128] O_2[129] and SOx.[130]

Monitoring and detection of gases is of most importance for emissions, toxic gas detection, and for process control. The development of high temperature gas sensors for industrial applications such as combustion processes is essential to improve energy efficiency and reduce toxic emissions.[131, 132]Gas sensors operating at high temperatures up to 1000 °C typically encounter many challenging issues, such as thermal stability. Composite material of Ce as Ceria-Zirconia has been investigated for temperature compensating materials for resistive oxygen sensor in lean-burn engines. The composite works best as long-term thermally stable material which provides higher sensitivity, reproducibility and selectivity and is suitable for application in harsh environments. [133] Similarly, gas sensors which could operate at low temperature are also needed for portable and low power consumption sensors. CeNSs as NO_2 gas sensors effectively detect low concentrations of NO_2 at low temperature with high sensitivity for environmental monitoring. The nanorods array films of Ce-doped ZnO on Al_2O_3 substrates with Pt spiral electrodes provide low operation temperature NO_2 sensors by undergoing a rapid and repeatable redox cycles. Ce doping not only improves the sensor response to NO_2, but also reduce the operating temperature. [134]A screen-printed potentiometric electrodes based on CeO_2 oxides has been constructed for monitoring the pH of Callovo─Oxfordian formation (COx), a candidate for nuclear waste storage. The electrochemical behavior of CeO_2based screen-printed electrodes (CeO_2-based SPEs) was determined by cyclic voltammetry and electrochemical impedance spectroscopy. The electrochemical behavior of CeO_2-based electrode showed superior electrochemical sensors that can affectively be used without the need for high input impedance equipment. [135]CeNSs has also emerged as an attractive redox active material for solar thermo-chemical cycles that can split CO_2 and H_2O to produce a mixture of CO and H_2 (syngas). The H_2O/CO_2-splitting in solar thermochemical cycle based on oxygen-deficient ceria that occurs in two-step.[136, 137] At high-temperature endothermic step, ceria is thermally reduced to a non-stoichiometric state using concentrated solar energy. In the subsequent, lower temperature exothermic step, ceria is re-oxidized with H_2O and/or CO_2 to produce H_2 and/or CO, respectively. The effective efficiency for splitting CO_2 and H_2O of solvothermal chemical cycles increases due to CeNSs unique property for existing in dual states. [138]

In order to get synergistic effect of ceria and cerium nitride, ceria nanorods hybrid with cerium nitride has been synthesized by providing ammonia environment and high temperature treatment. Interfacial junction between ceria and cerium nitride offers elevated electron transfer due to which catalytic activity is enhanced.[139] As a result, hybrid ceria rods demonstrated high photo-thermocatalysis of MB and phenol degradation and outstanding stability.[140]In last decade, many ceria based nanocomposites with Nobel metals have been synthesized to degrade hazardous formaldehyde. Recent research has unveiled that Nobel metal like Au, Pt based microporous nanocomposites with ceria offer 100% efficiency in formaldehyde photo-degradation at low temperature. Due to preciousness of Nobel metals, 1D ceria and Titania nanowires have been designed. In comparison to large volume nanomaterials, nanowires provides larger active surface area and lower diffusivity path to charge transfer hence clutched extreme potential for catalysis. As-synthesized CeO_2/TiO_2 nanowires showed 60.2% conversion at 60 ºC. Nanowires have superb long-term cycle stability showed no catalytic activity loss after 100 hours, also exhibited good photo-conversion of toluene.[141]

Oxygen storage capacity (OSC) of CeO_2also play vital role in photocatalytic activity. OSC can be increased by defect chemistry. In order to increase defects, CeO_2 nanosheets doped with Eu are prepared for photo-degradation of formaldehyde. As a result, as synthesized 4% Eu-doped CeO_2 nanosheets exhibit outstanding performance in photo-degradation of HCHO at low temperature of 120 ºC as well as remarkably enhanced photo-catalysis for HCHO gas degradation under ultra-violet exposure. Moreover, it offered high cycle stability for catalytic oxidation and photo-degradation.[65]BiOI supported CeO_2 nanosheets are prepared and analyzed for photocatalytic activity and O_2 gas evolution. Nanosheets offered enhanced surface area for BiOI to deposit which provided large numbers of defects on surface. Among varying %age of BiOI, 40% by weight supported CeO_2 nanosheets exhibited 89% elimination of rhodamine blue (RhB) dye (Fig.13) and generated 323×10^{-3} mM of O_2 in 2 hours.[142]

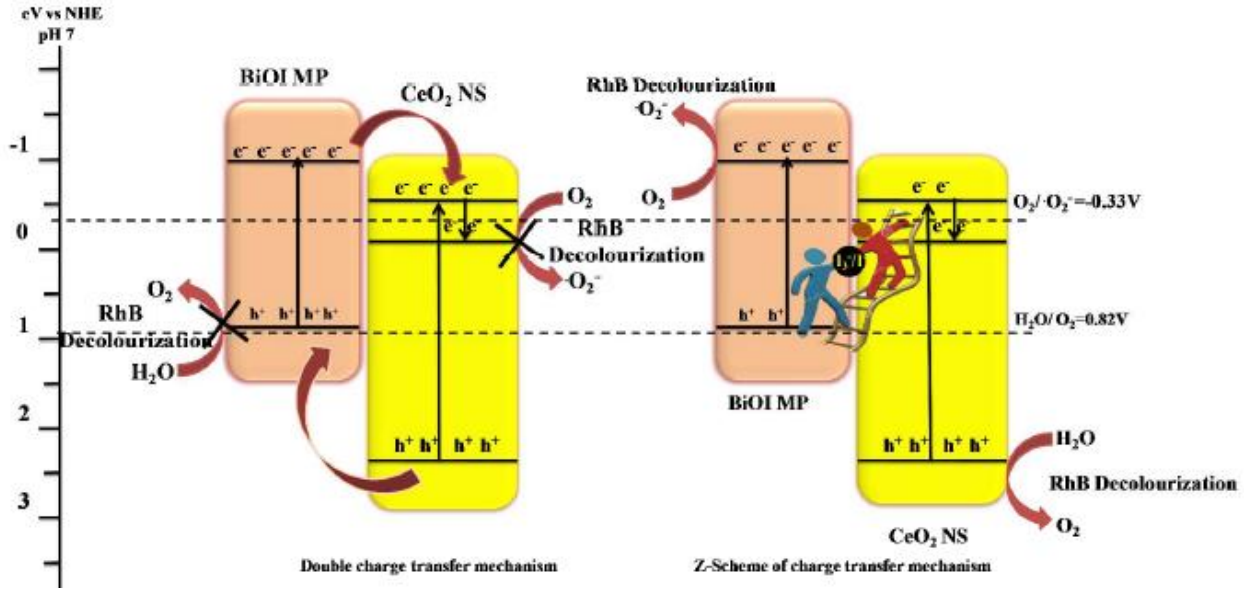

Fig. 13 Mechanism for catalytic degradation of RhB. Reproduced from ref. 142 with permission from American Chemical Society, 2017.

5. Conclusion and Future Perspectives

Ceria nanomaterials have received attraction in the past decade due to their promising applications in the fields of energy, biomedical and pharmaceutical, environment and in industry. Ceria nanostructures gained such an attention due to their unique size, shapes and crystallographic, optical, electrical and redox active behaviors. To improve the properties of the Ceria nanostructures in terms of their applications, an enormous number of reaction mechanisms and synthetic procedures have been designed. Various experimental conditions, including time, temperature, additive, pH value and concentration for the growth of CeO_2 nanocrystals were investigated as consistent annealing in hydrothermal synthesis produces, nanorods of cerium oxide with high oxygen defects. In surfactant and capping agent assisted synthesis, the shape and morphology change as we change the concentration of surfactant or capping agents. Microwave assisted synthesis controls the shape conversion by varying the temperature. Initial precursor concentration and types also play vital role in generation of variety in morphology and size of nanomaterials via adopting precursor and activator assisted synthesis. The methods, we described earlier, utilize organic or inorganic additive to generate various CeNSs with variety of morphology, shape, size and facet features. In order to avoid the contamination, caused by addition and sequential elimination of these additives, we commonly follow the template- free hydrothermal

method. The high potential of cerium aqueous solution to form coordination complex have utilized in screening, sensing and studying different applications in many areas. Due to improved structural, mechanical, and electrical properties with high biocompatibility and non-toxicity make CeNSs suitable material for making bio-electrodes. These bio-electrodes have been used to screen sense and study the various biomolecules including glucose, enzyme, amino acids, proteins, nucleotides, DNA and RNA with high selectivity, specificity and sensitivity. Due to dual oxidation state of CeNSs executes the free radical and reactive oxygen scavenging activity. Therefore, CeNSs and their composites have been applied to detect cancer biomarkers and in treatment of disorders caused by ROSs and radiation damage. Furthermore, due to redox activeness, oxygen rummaging capacity and high thermal stability of cerium nanomaterials, they have been played a vital role in environmental, industrial and energy applications like removal of hydrogen peroxide, MG and COD from water, sensing of toxic gases, increase in solvothermal reaction and energy storage devices. Therefore, an overview in this article provides a comprehensive understanding for designing new ceria based nanostructures with the desired properties for wide spread applications. Monitoring of the cerium oxide nanoparticles in precise time in the course of a desired cellular framework in vitro presents the predominant understanding needed to make the system a possible remedy for maladies involving unmediated ROS generation. Up conversion luminescence of CeNSs is expected to be possible in aqueous media by way of encapsulation or through synthesizing cerium oxide as a shell surrounding a strongly up converting luminescent center. The cerium oxide nanoparticle treatment is likely to be achievable via cellular systems *in vivo*. The advancement of *in vivo* studies demand progresses in targeting and extra studies into the prolonged-time period effects of containing these nanomaterials within the cellular system.

Quite a few efforts have been made to devise an ultrasensitive biosensor for studying bio-molecules like proteins, amino acids, enzymes, DNA and glucose devoid of interference from other redox-active species. With the help of nanotechnology, it is become possible to develop highly sensitive devices to study biomolecules at molecular level to some degree. Since CeNSs have mainly large surface-to-volume ratio, high IEP values and offer a better surface for enzyme immobilization, scientists have paid much considerations to these electrode materials in anticipation of highly stable, highly sensitive excluding less interfering free bio-molecules study. To make use of nanostructures for the treatment of diseases is an exciting domain of biomedical research, the promising potential for which has so far to be discerned. Current *in vitro* and *in vivo*

study has revealed that CeO_2 nanoparticles may grasp pledge for the remediationof disorders that are related with enhancement in tissue oxidative stress by ROS and inflammation. In upcoming years CeNSs may be promising therapeutic material for the disorders suffered from oxidative stress and inflammation. In the future CeNSs will deliver more significant contribution in energy transformation and storage devices (e.g. fuel cell and renewable fuel from solar energy, lithium-air batteries), green protection and remediation (e.g. treatment of harmful pollutants) as well as new emerging domain of biomedical applications (e.g. antioxidant agent, free radical scavenging and immune assay).

ACKNOWLEDGEMENTS

Marie Skłodowska-Curie Actions COFUND Fellowship to Dr. Nisar Ahmed is gratefully acknowledged. We are also thankful to Higher Education Commission (HEC) of Pakistan for financial support and cooperation.

References

1. M. Pawar, T. Sendo, #x011F, S. dular and P. Gouma, *Journal of Nanomaterials*, 2018, **2018**, 13.
2. C. Xu and X. Qu, *NPG Asia Materials*, 2014, **6**, e90.
3. L. Malavasi, C. A. J. Fisher and M. S. Islam, *Chemical Society Reviews*, 2010, **39**, 4370-4387.
4. M. V. Ganduglia-Pirovano, A. Hofmann and J. Sauer, *Surface Science Reports*, 2007, **62**, 219-270.
5. J. T. Dahle and Y. Arai, *International Journal of Environmental Research and Public Health*, 2015, **12**, 1253-1278.
6. T. Pirmohamed, J. M. Dowding, S. Singh, B. Wasserman, E. Heckert, A. S. Karakoti, J. E. S. King, S. Seal and W. T. Self, *Chem Commun*, 2010, **46**, 2736-2738.
7. E. G. Heckert, A. S. Karakoti, S. Seal and W. T. Self, *Biomaterials*, 2008, **29**, 2705-2709.
8. K. Kalantar-zadeh, J. Z. Ou, T. Daeneke, A. Mitchell, T. Sasaki and M. S. Fuhrer, *Applied Materials Today*, 2016, **5**, 73-89.
9. V. Baldim, F. Bedioui, N. Mignet, I. Margaill and J. F. Berret, *Nanoscale*, 2018, **10**, 6971-6980.
10. T. Montini, M. Melchionna, M. Monai and P. Fornasiero, *Chemical Reviews*, 2016, **116**, 5987-6041.
11. C. Walkey, S. Das, S. Seal, J. Erlichman, K. Heckman, L. Ghibelli, E. Traversa, J. F. McGinnis and W. T. Self, *Environmental Science: Nano*, 2015, **2**, 33-53.
12. W.-X. Tang and P.-X. Gao, *MRS Communications*, 2016, **6**, 311-329.
13. F. Corsi, F. Caputo, E. Traversa and L. Ghibelli, *Frontiers in oncology*, 2018, **8**.
14. A. Dhall and W. Self, *Antioxidants*, 2018, **7**, 97.
15. D. Carta, T. Montini, M. F. Casula, M. Monai, S. Bullita, P. Fornasiero and A. Corrias, *Journal of Materials Chemistry A*, 2017, **5**, 20024-20034.
16. L. Yue and X.-M. Zhang, *Journal of Alloys and Compounds*, 2009, **475**, 702-705.
17. N. P. Sardesai, D. Andreescu and S. Andreescu, *Journal of the American Chemical Society*, 2013, **135**, 16770-16773.
18. M. Mao, H. Lv, Y. Li, Y. Yang, M. Zeng, N. Li and X. Zhao, *ACS Catalysis*, 2015, **6**, 418-427.
19. J. M. López, A. L. Gilbank, T. García, B. Solsona, S. Agouram and L. Torrente-Murciano, *Applied Catalysis B: Environmental*, 2015, **174**, 403-412.
20. R. Wang and M. Fang, *Journal of Materials Chemistry*, 2012, **22**, 1770-1773.
21. H. Pang and C. Chen, *RSC Advances*, 2014, **4**, 14872-14878.
22. X. Xia, Q. Hao, W. Lei, W. Wang, D. Sun and X. Wang, *Journal of Materials Chemistry*, 2012, **22**, 16844-16850.
23. I. Vladimirov, M. Kellermeier, T. Geßner, Z. Molla, S. Grigorian, U. Pietsch, L. S. Schaffroth, M. Kühn, F. May and R. T. Weitz, *Nano letters*, 2017, **18**, 9-14.
24. C. Xu, Y. Lin, J. Wang, L. Wu, W. Wei, J. Ren and X. Qu, *Advanced healthcare materials*, 2013, **2**, 1591-1599.
25. Y. C. Zhou, R. J. Phillips and J. A. Switzer, *J Am Ceram Soc*, 1995, **78**, 981-985.
26. E. Verdon, M. Devalette and G. Demazeau, *Mater Lett*, 1995, **25**, 127-131.
27. Q. G. Dai, S. X. Bai, H. Li, W. Liu, X. Y. Wang and G. Z. Lu, *Crystengcomm*, 2014, **16**, 9817-9827.

28. T. Masui, K. Fujiwara, K. Machida, G. Adachi, T. Sakata and H. Mori, *Chem Mater*, 1997, **9**, 2197-2204.
29. A. A. Ansari, P. R. Solanki and B. D. Malhotra, *Appl Phys Lett*, 2008, **92**.
30. V. D. Araujo, W. Avansi, H. B. de Carvalho, M. L. Moreira, E. Longo, C. Ribeiro and M. I. B. Bernardi, *Crystengcomm*, 2012, **14**, 1150-1154.
31. D. S. Zhang, H. X. Fu, L. Y. Shi, C. S. Pan, Q. Li, Y. L. Chu and W. J. Yu, *Inorg Chem*, 2007, **46**, 2446-2451.
32. J. M. Perez, A. Asati, S. Nath and C. Kaittanis, *Small*, 2008, **4**, 552-556.
33. S. Phoka, P. Laokul, E. Swatsitang, V. Promarak, S. Seraphin and S. Maensiri, *Mater Chem Phys*, 2009, **115**, 423-428.
34. G. Wang, Q. Mu, T. Chen and Y. Wang, *Journal of Alloys and Compounds*, 2010, **493**, 202-207.
35. S. Wang, L. Zhao, W. Wang, Y. Zhao, G. Zhang, X. Ma and J. Gong, *Nanoscale*, 2013, **5**, 5582-5588.
36. J. M. Perez, A. Asati, S. Nath and C. Kaittanis, *Small*, 2008, **4**, 552-556.
37. G. Wang, Q. Mu, T. Chen and Y. Wang, *Journal of Alloys and Compounds*, 2010, **493**, 202-207.
38. S. K. Ujjain, A. Das, G. Srivastava, P. Ahuja, M. Roy, A. Arya, K. Bhargava, N. Sethy, S. K. Singh and R. K. Sharma, *Biointerphases*, 2014, **9**, 031011.
39. E. Verdon, M. Devalette and G. Demazeau, *Materials letters*, 1995, **25**, 127-131.
40. T. Masui, K. Fujiwara, K.-i. Machida, G.-y. Adachi, T. Sakata and H. Mori, *Chemistry of Materials*, 1997, **9**, 2197-2204.
41. W. Wang, J. Y. Howe, Y. Li, X. Qiu, D. C. Joy, M. P. Paranthaman, M. J. Doktycz and B. Gu, *Journal of Materials Chemistry*, 2010, **20**, 7776-7781.
42. Q. Wu, F. Zhang, P. Xiao, H. Tao, X. Wang, Z. Hu and Y. Lu, *The Journal of Physical Chemistry C*, 2008, **112**, 17076-17080.
43. Z.-L. Wang, G.-R. Li, Y.-N. Ou, Z.-P. Feng, D.-L. Qu and Y.-X. Tong, *The Journal of Physical Chemistry C*, 2011, **115**, 351-356.
44. T. S. Sakthivel, D. L. Reid, U. M. Bhatta, G. Mobus, D. C. Sayle and S. Seal, *Nanoscale*, 2015, **7**, 5169-5177.
45. E.-J. Park, J. Choi, Y.-K. Park and K. Park, *Toxicology*, 2008, **245**, 90-100.
46. F. Zhang, Q. Jin and S. W. Chan, *J Appl Phys*, 2004, **95**, 4319-4326.
47. O. Polezhaeva, N. Yaroshinskaya and V. Ivanov, *Inorganic Materials*, 2008, **44**, 51-57.
48. T. D. Nguyen, C. T. Dinh, D. Mrabet, M. N. Tran-Thi and T. O. Do, *J Colloid Interf Sci*, 2013, **394**, 100-107.
49. S. K. Ujjain, A. Das, G. Srivastava, P. Ahuja, M. Roy, A. Arya, K. Bhargava, N. Sethy, S. K. Singh, R. K. Sharma and M. Das, *Biointerphases*, 2014, **9**.
50. S. Deshpande, S. Patil, S. V. N. T. Kuchibhatla and S. Seal, *Appl Phys Lett*, 2005, **87**.
51. J. Y. Ying and A. Tschope, *Chem Eng J*, 1996, **64**, 225-237.
52. Q. Wu, F. Zhang, P. Xiao, H. S. Tao, X. Z. Wang, Z. Hu and Y. N. Lu, *J Phys Chem C*, 2008, **112**, 17076-17080.
53. W. Wang, J. Y. Howe, Y. A. Li, X. F. Qiu, D. C. Joy, M. P. Paranthaman, M. J. Doktycz and B. H. Gu, *J Mater Chem*, 2010, **20**, 7776-7781.
54. C. S. Pan, D. S. Zhang, L. Y. Shi and J. H. Fang, *Eur J Inorg Chem*, 2008, DOI: 10.1002/ejic.200800047, 2429-2436.
55. H. L. Lin, C. Y. Wu and R. K. Chiang, *J Colloid Interf Sci*, 2010, **341**, 12-17.

56. H.-X. Mai, L.-D. Sun, Y.-W. Zhang, R. Si, W. Feng, H.-P. Zhang, H.-C. Liu and C.-H. Yan, *The Journal of Physical Chemistry B*, 2005, **109**, 24380-24385.
57. Z. Ji, X. Wang, H. Zhang, S. Lin, H. Meng, B. Sun, S. George, T. Xia, A. E. Nel and J. I. Zink, *Acs Nano*, 2012, **6**, 5366-5380.
58. H. X. Mai, L. D. Sun, Y. W. Zhang, R. Si, W. Feng, H. P. Zhang, H. C. Liu and C. H. Yan, *J Phys Chem B*, 2005, **109**, 24380-24385.
59. R. Yu, L. Yan, P. Zheng, J. Chen and X. R. Xing, *J Phys Chem C*, 2008, **112**, 19896-19900.
60. L. Yan, R. B. Yu, J. Chen and X. R. Xing, *Cryst Growth Des*, 2008, **8**, 1474-1477.
61. R. Si and M. Flytzani-Stephanopoulos, *Angew Chem Int Edit*, 2008, **47**, 2884-2887.
62. M. Yamashita, K. Kameyama, S. Yabe, S. Yoshida, Y. Fujishiro, T. Kawai and T. Sato, *Journal of materials science*, 2002, **37**, 683-687.
63. M.-S. Tsai, *Materials Science and Engineering: B*, 2004, **110**, 132-134.
64. X.-D. Zhou, W. Huebner and H. Anderson, *Applied physics letters*, 2002, **80**, 3814.
65. Y. Huang, B. Long, M. Tang, Z. Rui, M.-S. Balogun, Y. Tong and H. Ji, *Applied Catalysis B: Environmental*, 2016, **181**, 779-787.
66. X.-h. Lu, X. Huang, S.-l. Xie, D.-z. Zheng, Z.-q. Liu, C.-l. Liang and Y.-X. Tong, *Langmuir*, 2010, **26**, 7569-7573.
67. I. Yamaguchi, M. Watanabe, T. Shinagawa, M. Chigane, M. Inaba, A. Tasaka and M. Izaki, *ACS applied materials & interfaces*, 2009, **1**, 1070-1075.
68. O. S. Hammond, K. J. Edler, D. T. Bowron and L. Torrente-Murciano, *Nature Communications*, 2017, **8**, 14150.
69. K. Reed, A. Cormack, A. Kulkarni, M. Mayton, D. Sayle, F. Klaessig and B. Stadler, *Environmental Science: Nano*, 2014, **1**, 390-405.
70. M. Aryanpour, A. Khetan and H. Pitsch, *ACS Catalysis*, 2013, **3**, 1253-1262.
71. D. R. Mullins, *Surface Science Reports*, 2015, **70**, 42-85.
72. A. Migani, G. N. Vayssilov, S. T. Bromley, F. Illas and K. M. Neyman, *Chemical Communications*, 2010, **46**, 5936-5938.
73. T. X. T. Sayle, F. Caddeo, X. Zhang, T. Sakthivel, S. Das, S. Seal, S. Ptasinska and D. C. Sayle, *Chemistry of Materials*, 2016, **28**, 7287-7295.
74. S. D. Park, J. M. Vohs and R. J. Gorte, *Nature*, 2000, **404**, 265-267.
75. T. Hibino, A. Hashimoto, T. Inoue, J. Tokuno, S. Yoshida and M. Sano, *Science*, 2000, **288**, 2031-2033.
76. W. C. Chueh, C. Falter, M. Abbott, D. Scipio, P. Furler, S. M. Haile and A. Steinfeld, *Science*, 2010, **330**, 1797-1801.
77. A. Kaushik, P. R. Solanki, M. K. Pandey, S. Ahmad and B. D. Malhotra, *Appl Phys Lett*, 2009, **95**.
78. O. Estevez-Hernadndez, J. L. H. H. de Cisneros, E. Reguera and I. Naranjo-Rodriguez, *Sensor Actuat B-Chem*, 2007, **120**, 766-772.
79. A. Wei, X. W. Sun, J. X. Wang, Y. Lei, X. P. Cai, C. M. Li, Z. L. Dong and W. Huang, *Appl Phys Lett*, 2006, **89**.
80. R. K. Shervedani, A. H. Mehrjardi and N. Zamiri, *Bioelectrochemistry*, 2006, **69**, 201-208.
81. A. Heller and B. Feldman, *Chemical reviews*, 2008, **108**, 2482-2505.
82. S. Saha, S. K. Arya, S. P. Singh, K. Sreenivas, B. D. Malhotra and V. Gupta, *Biosens Bioelectron*, 2009, **24**, 2040-2045.
83. A. A. Ansari, M. Azahar and B. D. Malhotra, *India-Japan Workshop on Biomolecular Electronics and Organic Nanotechnology for Environment Preservation*, 2012, **358**.

84. A. Kaushik, P. R. Solanki, A. A. Ansari, S. Ahmad and B. D. Malhotra, *Nanotechnology*, 2009, **20**.
85. Y. Y. Chu, Z. B. Wang, Z. Z. Jiang, D. M. Gu and G. P. Yin, *Adv Mater*, 2011, **23**, 3100-+.
86. J. D. Qiu, S. G. Cui and R. P. Liang, *Microchim Acta*, 2010, **171**, 333-339.
87. X. H. Pang, J. X. Li, Y. B. Zhao, D. Wu, Y. Zhang, B. Du, H. M. Ma and Q. Wei, *Acs Appl Mater Inter*, 2015, **7**, 19260-19267.
88. J. Peng, Y. D. Zhu, X. H. Li, L. P. Jiang, E. S. Abdel-Halim and J. J. Zhu, *Microchim Acta*, 2014, **181**, 1505-1512.
89. H. P. Zhou, J. Y. Xi, Z. H. Li, Z. Y. Zhang, L. H. Yu, L. Liu, X. P. Qiu and L. Q. Chen, *Rsc Adv*, 2014, **4**, 61912-61918.
90. M. Hosseini, M. R. K. Pur, P. Norouzi, M. R. Moghaddam, F. Faridbod, M. R. Ganjali and J. Shamsi, *Anal Methods-Uk*, 2015, **7**, 1936-1942.
91. L. Li, Y. Wang, L. Pan, Y. Shi, W. Cheng, Y. Shi and G. Yu, *Nano letters*, 2015, **15**, 1146-1151.
92. Y. Wei, M. G. Li and B. Fang, *Chinese J Chem*, 2007, **25**, 1622-1626.
93. Y. W. Yao, L. M. Jiao, L. H. Cui, N. C. Yu, F. Wei and Z. M. Lu, *J Electrochem Soc*, 2015, **162**, H693-H698.
94. S. S. Lee, W. Song, M. Cho, H. L. Puppala, P. Nguyen, H. Zhu, L. Segatori and V. L. Colvin, *ACS nano*, 2013, **7**, 9693-9703.
95. C. M. Rico, J. Hong, M. I. Morales, L. Zhao, A. C. Barrios, J.-Y. Zhang, J. R. Peralta-Videa and J. L. Gardea-Torresdey, *Environmental science & technology*, 2013, **47**, 5635-5642.
96. I. Celardo, J. Z. Pedersen, E. Traversa and L. Ghibelli, *Nanoscale*, 2011, **3**, 1411-1420.
97. S. M. Hirst, A. Karakoti, S. Singh, W. Self, R. Tyler, S. Seal and C. M. Reilly, *Environmental toxicology*, 2013, **28**, 107-118.
98. J. L. Niu, A. Azfer, L. M. Rogers, X. H. Wang and P. E. Kolattukudy, *Cardiovasc Res*, 2007, **73**, 549-559.
99. D. Schubert, R. Dargusch, J. Raitano and S. W. Chan, *Biochem Bioph Res Co*, 2006, **342**, 86-91.
100. R. W. Tarnuzzer, J. Colon, S. Patil and S. Seal, *Nano Lett*, 2005, **5**, 2573-2577.
101. C. Korsvik, S. Patil, S. Seal and W. T. Self, *Chem Commun*, 2007, DOI: 10.1039/b615134e, 1056-1058.
102. C. Xu and X. G. Qu, *Npg Asia Materials*, 2014, **6**.
103. M. Ornatska, E. Sharpe, D. Andreescu and S. Andreescu, *Anal Chem*, 2011, **83**, 4273-4280.
104. X. Jiao, H. J. Song, H. H. Zhao, W. Bai, L. C. Zhang and Y. Lv, *Anal Methods-Uk*, 2012, **4**, 3261-3267.
105. X. Wang, D. Zhang, Y. Li, D. Tang, Y. Xiao, Y. Liu and Q. Huo, *RSC Advances*, 2013, **3**, 3623-3630.
106. A. Karakoti, S. Singh, J. M. Dowding, S. Seal and W. T. Self, *Chem Soc Rev*, 2010, **39**, 4422-4432.
107. P. E. Kolattukudy, T. Quach, S. Bergese, S. Breckenridge, J. Hensley, R. Altschuld, G. Gordillo, S. Klenotic, C. Orosz and J. Parker-Thornburg, *Am J Pathol*, 1998, **152**, 101-111.
108. C. W. Younce, K. K. Wang and P. E. Kolattukudy, *Cardiovasc Res*, 2010, **87**, 665-674.
109. A. Asati, C. Kaittanis, S. Santra and J. M. Perez, *Anal Chem*, 2011, **83**, 2547-2553.

110. P. X. Zhao, Y. Zhao, X. F. Guo, H. Wang and H. S. Zhang, *J Chromatogr A*, 2011, **1218**, 2528-2539.
111. G.-T. Zhu, X.-M. He, X. Chen, D. Hussain, J. Ding and Y.-Q. Feng, *Journal of Chromatography A*, 2016, **1437**, 137-144.
112. D. Hussain, S. G. Musharraf and M. Najam-ul-Haq, *Analytical and bioanalytical chemistry*, 2016, **408**, 1633-1641.
113. B. Fatima, M. Najam-ul-Haq, F. Jabeen, S. Majeed, M. N. Ashiq, S. G. Musharraf, B. A. Shad and G. B. Xu, *Analyst*, 2013, **138**, 5059-5067.
114. B. D'Angelo, S. Santucci, E. Benedetti, S. Di Loreto, R. A. Phani, S. Falone, F. Amicarelli, M. P. Ceru and A. Cimini, *Curr Nanosci*, 2009, **5**, 167-176.
115. R. A. Madero-Visbal, B. E. Alvarado, J. F. Colon, C. H. Baker, M. S. Wason, B. Isley, S. Seal, C. M. Lee, S. Das and R. Manon, *Nanomed-Nanotechnol*, 2012, **8**, 1223-1231.
116. J. Colon, N. Hsieh, A. Ferguson, P. Kupelian, S. Seal, D. W. Jenkins and C. H. Baker, *Nanomed-Nanotechnol*, 2010, **6**, 698-705.
117. C. K. Kim, T. Kim, I. Y. Choi, M. Soh, D. Kim, Y. J. Kim, H. Jang, H. S. Yang, J. Y. Kim, H. K. Park, S. P. Park, S. Park, T. Yu, B. W. Yoon, S. H. Lee and T. Hyeon, *Angew Chem Int Edit*, 2012, **51**, 11039-11043.
118. K. Nikolaou, *Sci Total Environ*, 1999, **235**, 71-76.
119. T. X. T. Sayle, S. C. Parker and D. C. Sayle, *Phys Chem Chem Phys*, 2005, **7**, 2936-2941.
120. N. Shehata, M. Azab, I. Kandas and K. Meehan, *Sensors-Basel*, 2015, **15**, 20193-20203.
121. Y. Yao, L. Jiao, L. Cui, N. Yu, F. Wei and Z. Lu, *Journal of The Electrochemical Society*, 2015, **162**, H693-H698.
122. Y. Tang, Y. Yang, D. Cheng, B. Gao, Y. Wan and Y. C. Li, *ACS Sustainable Chemistry & Engineering*, 2017, **5**, 10099-10110.
123. K. Deori, C. Kalita and S. Deka, *Journal of Materials Chemistry A*, 2015, **3**, 6909-6920.
124. A. Trovarelli, *Catalysis Reviews*, 1996, **38**, 439-520.
125. J. Hu, C. Zou, Y. Su, M. Li, X. Ye, B. Cai, E. S.-W. Kong, Z. Yang and Y. Zhang, *Sensors and Actuators B: Chemical*, 2018, **270**, 119-129.
126. E. Laubender, N. Tanvir, G. Urban and O. Yurchenko, *Materials Today: Proceedings*, 2016, **3**, 429-433.
127. D. E. Motaung, G. H. Mhlongo, P. R. Makgwane, B. P. Dhonge, F. R. Cummings, H. C. Swart and S. S. Ray, *Sensors and Actuators B: Chemical*, 2018, **254**, 984-995.
128. A. Katoch, J.-H. Kim, Y. J. Kwon, H. W. Kim and S. S. Kim, *ACS applied materials & interfaces*, 2015, **7**, 11351-11358.
129. L. Zhang, Q. Fang, Y. Huang, K. Xu, P. K. Chu and F. Ma, *Analytical chemistry*, 2018, **90**, 9821-9829.
130. J. Liu, M. Dai, T. Wang, P. Sun, X. Liang, G. Lu, K. Shimanoe and N. Yamazoe, *ACS applied materials & interfaces*, 2016, **8**, 6669-6677.
131. J. Kašpar, P. Fornasiero and N. Hickey, *Catalysis Today*, 2003, **77**, 419-449.
132. M. Shelef and R. W. McCabe, *Catalysis Today*, 2000, **62**, 35-50.
133. R. Moos, N. Izu, F. Rettig, S. Reiss, W. Shin and I. Matsubara, *Sensors-Basel*, 2011, **11**, 3439-3465.
134. C. J. Chang, C. Y. Lin, J. K. Chen and M. H. Hsu, *Ceram Int*, 2014, **40**, 10867-10875.
135. S. Betelu, K. Polychronopoulou, C. Rebholz and I. Ignatiadis, *Talanta*, 2011, **87**, 126-135.
136. J. R. Scheffe, M. Welte and A. Steinfeld, *Industrial & Engineering Chemistry Research*, 2014, **53**, 2175-2182.

137. P. Furler, J. Scheffe, M. Gorbar, L. Moes, U. Vogt and A. Steinfeld, *Energy & Fuels*, 2012, **26**, 7051-7059.
138. P. Furler, J. R. Scheffe and A. Steinfeld, *Energ Environ Sci*, 2012, **5**, 6098-6103.
139. C. T. Campbell and C. H. F. Peden, *Science*, 2005, **309**, 713.
140. Y. Huang, Y. Lu, Y. Lin, Y. Mao, G. Ouyang, H. Liu, S. Zhang and Y. Tong, *Journal of Materials Chemistry A*, 2018.
141. Y. Huang, H. Li, M.-S. Balogun, H. Yang, Y. Tong, X. Lu and H. Ji, *RSC Advances*, 2014, **5**, 7729-7733.
142. S. Sultana, S. Mansingh and K. Parida, *The Journal of Physical Chemistry C*, 2017, **122**, 808-819.